

# Catalysis Science & Technology

Accepted Manuscript



This is an *Accepted Manuscript*, which has been through the Royal Society of Chemistry peer review process and has been accepted for publication.

*Accepted Manuscripts* are published online shortly after acceptance, before technical editing, formatting and proof reading. Using this free service, authors can make their results available to the community, in citable form, before we publish the edited article. We will replace this *Accepted Manuscript* with the edited and formatted *Advance Article* as soon as it is available.

You can find more information about *Accepted Manuscripts* in the [Information for Authors](#).

Please note that technical editing may introduce minor changes to the text and/or graphics, which may alter content. The journal's standard [Terms & Conditions](#) and the [Ethical guidelines](#) still apply. In no event shall the Royal Society of Chemistry be held responsible for any errors or omissions in this *Accepted Manuscript* or any consequences arising from the use of any information it contains.



Journal Name

ARTICLE

## Highly selective hydrogenation of $\alpha$ , $\beta$ -unsaturated aldehydes by Pt catalysts supported on Fe-based layered double hydroxides and derived mixed metal oxides

Received 00th January 20xx,  
Accepted 00th January 20xx

DOI: 10.1039/x0xx00000x

Zhengbin Tian<sup>†</sup>, Qingyang Li<sup>†</sup>, Juying Hou, Yan Li<sup>\*</sup>, Shiyun Ai<sup>\*</sup>

www.rsc.org/

The selective hydrogenation of cinnamaldehyde and citral was investigated over Fe-based layered double hydroxides and derived mixed metal oxides supported Platinum catalysts. Among the catalysts, Pt/ZnFe-LDH showed the best activity and selectivity for the hydrogenation of C=O bond in the cinnamaldehyde and citral was mostly transformed into citronellol over the Pt/NiFe-LDH catalyst.

Selective hydrogenation of  $\alpha$ ,  $\beta$ -unsaturated aldehydes to unsaturated alcohols is of great importance in pharmaceutical and fragrance industries.<sup>1</sup> Also, it is considered as a good model used for investing the catalytic behaviors of the microstructures of heterogeneous catalysts. Cinnamaldehyde (CAL) and citral are two particularly important representatives of  $\alpha$ ,  $\beta$ -unsaturated aldehyde. Particularly, an isolated double bond (C=C) exist in citral except a conjugate double bond (C=C) and a carbonyl group (C=O).<sup>2</sup> The selective hydrogenation is a rather complex reaction network involving several important intermediates and a number of series-parallel reactions (Fig. S1, Fig. S2). Over the past few years, many researchers have been devoted to performing liquid phase selective hydrogenation of citral and CAL over a variety of supported nano-sized noble metal catalysts (e.g. Pd, Pt, Ru and Au).<sup>2-5</sup> However, obtaining the unsaturated alcohols is difficult since the hydrogenation of the C=C bond, owing to the fact that the C=O bond presents a higher binding energy than the bond C=C,<sup>6</sup> the reduction of the C=C bond is thermodynamically more favorable than that of C=O bond.

Many studies have been devoted to enhance the selectivity towards the unsaturated alcohol either by fine control of the sizes<sup>7</sup> and/or the exposed facets of the active metal nanoparticles,<sup>8</sup> or by exploiting the steric constraints imposed by the environment of the active site,<sup>9</sup> or by decorating the

primary metal with a second metal component.<sup>10</sup> It is well known there is an interaction (e.g. strong metal-support interaction effect (SMSI effect)) between the support and active metal sites that can modify the catalytic properties of the metal catalyst. It is a feasible way to search for appropriate materials used as catalyst supports for preparing highly active and selective catalysts for the selective hydrogenation of unsaturated aldehydes. Guo et al.<sup>9</sup> reported the cavities of an amino-functionalized Zr-terephthalate metal-organic framework confined Pt nanoclusters catalyst for the hydrogenation of CAL. The steric effect of support was used to restrict the C=C in the middle of a long molecule from easily adsorbing onto the surface of Pt nanoparticles, resulting in a high selectivity to unsaturated alcohols. Concepción et al.<sup>11</sup> researched the promotional effect of Sn-beta zeolites supported platinum catalyst for the citral, showing that the effect of a Lewis acid site and the steric effects induced by zeolite channels had an significant impact on the reaction.

Layered double hydroxides (LDH) are a class of synthetic highly ordered two-dimensional anionic clays consisting of positively charged layers (divalent and trivalent cations) with charge-balancing anions (expressed as  $[M_x^{1+2+}M_x^{3+}(\text{OH})_2](A^{n-})_{x/n} \cdot m\text{H}_2\text{O}$ ), which can be widely employed as promising

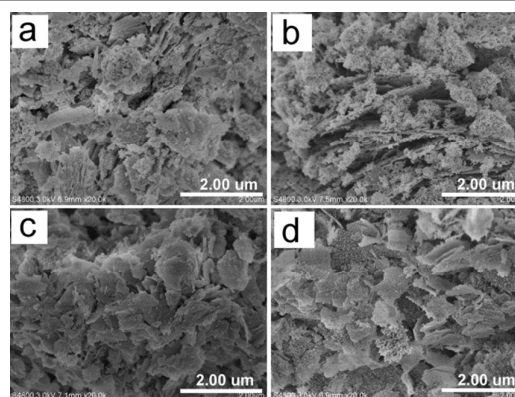


Fig. 1 SEM images of (a) ZnFe-LDH, (b) ZnFe-MMO, (c) NiFe-LDH and (d) NiFe-MMO.

College of Chemistry and Material Science, Shandong Agricultural University, 271018, Taian, Shandong, PR China

<sup>†</sup> These authors contributed equal to this work.

E-mail address: liyan2010@sda.u.edu.cn (Yan Li); ashy@sda.u.edu.cn (Shiyun Ai)  
Fax: 86-538-8242251.

Electronic Supplementary Information (ESI) available: [details of any supplementary information available should be included here]. See DOI: 10.1039/x0xx00000x

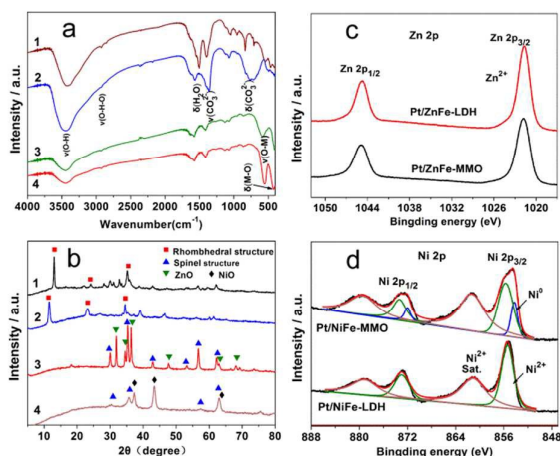


**Fig. 2** (a) FTIR and (b) XRD patterns of (1) ZnFe-LDH, (2) ZnFe-MMO, (3) NiFe-LDH and (4) NiFe-MMO; (c), Zn2p spectrum; (d) Ni2p spectrum.

heterogeneous catalysts and supports.<sup>12, 13</sup> The mixed metal oxides (MMO) derived from LDH are also applying in various areas due to their excellent properties.<sup>14, 15</sup> Xiang et al.<sup>13</sup> reported that the hydroxyl group in the MgAl-LDH structure may inhibit the adsorption of the C=C bond by electrostatically repelling the phenyl ring of CAL. In our previous research, we investigated a series of Al-based LDH (divalent metal: Co, Ni, Zn, Mg) and corresponding MMO supported Pt catalyst for the selective hydrogenation of CAL.<sup>16</sup> We found that CoAl-LDH and derived MMO supported catalyst exhibited excellent conversion and ca. 75% selectivity to COL. Transition metal plays a significant role in the reaction. It has been demonstrated that the presence of high-valent ionic species ( $\text{Fe}^{\delta+}$ ,  $\text{Ge}^{\delta+}$ ,  $\text{Sn}^{\delta+}$ ) favours the activation of the carbonyl group.<sup>11, 17, 18</sup> We speculate that Fe-based LDH would show more excellent activity and better selectivity.

In this work, MFe-LDH (M=Co, Ni, Mg, Zn) was synthesized using a conventional coprecipitation method by the urea slow hydrolysis process and transformed into MFe-MMO after calcination at 450 °C for 4 h. The Pt catalysts were prepared using a reduction-deposition method and were tested in the hydrogenation reaction of CAL and citral under the same mild conditions for the investigation of the support effect, which was carried out in a stainless steel autoclave. The result has confirmed what we suspected.

The morphology of as-prepared samples was investigated by means of scanning electron microscopy (SEM). All the SEM images showed randomly oriented two-dimensional sheet-like shapes affording a rough surface as well as granular aggregates (Fig. 1). Apart from increasing of pore size, calcination effect almost had no change on the morphology.

Typical of FTIR spectrum (Fig. 2a) for the LDH is the strong and broad absorption band between 3600 and 3200  $\text{cm}^{-1}$  centered around 3450  $\text{cm}^{-1}$  corresponding to the O-H stretching vibrations of the hydroxyl groups in the hydroxyl layers and interlayer water molecules. The characteristic peaks attributable to the symmetric stretching vibrations and out-of-plane deformation of  $\text{CO}_3^{2-}$  are observed, suggestive of the presence of

**Table 1** Textural Properties of ZnFe-LDH, NiFe-LDH and derived MMO supported Pt catalysis

Catalysts	$S_{\text{BET}}^a$ ( $\text{m}^2/\text{g}$ )	$S_{\text{BJH}}^b$ ( $\text{m}^2/\text{g}$ )	$V_{\text{meso}}^b$ ( $\text{cm}^3/\text{g}$ )	$D_{\text{BJH}}^c$ (nm)
Pt/ZnFe-LDH	146.2	157.5	0.45	3.82
Pt/ZnFe-MMO	51.3	61.2	0.41	30.96
Pt/NiFe-LDH	63.6	70.6	0.26	12.37
Pt/NiFe-MMO	26.8	31.0	0.25	30.86

<sup>a</sup>  $S_{\text{BET}}$ : from the BET method; <sup>b</sup>  $S_{\text{BJH}}$  and  $V_{\text{meso}}$ : calculated from the BJH method; <sup>c</sup>  $D_{\text{BJH}}$ : mesopore diameter calculated from absorption branch of nitrogen isotherms using BJH method

interlayer carbonate anions.<sup>19</sup> After calcining LDH at 450 °C, the characteristic peaks representing  $\text{CO}_3^{2-}$  completely vanish and two obviously sharp peaks attributed to the enhanced M-O vibrations were presented, which implied that LDH had transformed into MMO with the absence of  $\text{CO}_3^{2-}$  and the attendance of large amount of M-O bond.<sup>20</sup> The measured XRD patterns (Fig. 2a) of the LDHs were fitted well to LDH rhombohedral structure with basal reflections of planes (003), (006), and (012).<sup>21</sup> The layered structure of the original LDHs was completely destroyed after calcination as no characteristic diffractions of LDHs were present in the XRD patterns for the calcined MMO. The XRD pattern also confirmed the formation of the mixture of the spinel structure and MO (N=Zn, Ni).

The  $\text{N}_2$  adsorption-desorption isotherms and corresponding pore size distribution of the as-prepared catalyst are shown in Fig. 3. All sorption isotherms exhibit mixed type II and IV behaviour with H3-type hysteresis loop. The H3 type hysteresis loop was related to aggregates of plate-like particles giving rise to slit-shaped pores. Table 1 summarizes the BET surface area and total pore volume calculated from the  $\text{N}_2$  adsorption-desorption isotherm. From Table 1, the BET surface areas and total pore volumes are 63.6  $\text{m}^2 \text{g}^{-1}$  and 0.26  $\text{cm}^3 \text{g}^{-1}$  for Pt/ZnFe-LDH, and 146.2  $\text{m}^2 \text{g}^{-1}$  and 0.45  $\text{cm}^3 \text{g}^{-1}$  for Pt/NiFe-LDH respectively. These values decrease to 26.8  $\text{m}^2 \text{g}^{-1}$  and 0.25  $\text{cm}^3 \text{g}^{-1}$  for Pt/ZnFe-MMO, and 51.3  $\text{m}^2 \text{g}^{-1}$  and 0.41  $\text{cm}^3 \text{g}^{-1}$  for Pt/NiFe-MMO, respectively, after calcination at 450 °C,

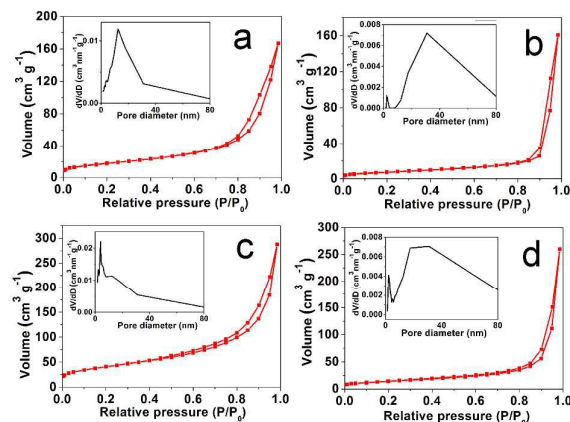


**Fig. 3** Nitrogen adsorption-desorption isotherms and corresponding pore size distribution curves (inset) of (a) ZnFe-LDH, (b) ZnFe-MMO, (c) NiFe-LDH and (d) NiFe-MMO.

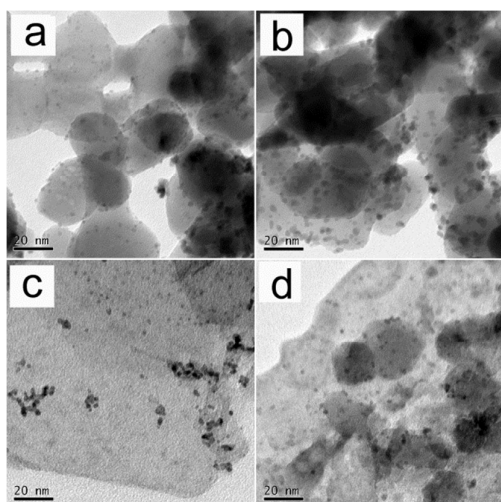


**Fig. 4** TEM images of (a) Pt/ZnFe-LDH, (b) Pt/ZnFe-MMO, (c) Pt/NiFe-LDH and (d) Pt/NiFe-MMO.

which were opposite to results observed in the Al-based MMO. It can be ascribed to the aggregates of larger MO ( $M = \text{Zn}$  and  $\text{Ni}$ ) particles, the breakage of mesopore network and the surface collapse of nanosheets to some extent. This was agreement with the SEM image and pore size distribution image. Vanishing of small-size pores and appearance of large-size pores showed the presence of the breakage and collapse. The specific surface area, pore volume and pore diameter of the catalyst is not the dominant factor in determining its activity, however, the lower specific surface area, such as for ZnFe-MMO, limited the effective exposure of active sites. We found that the size distribution of Pt NPs on the catalysts prepared with reduction-deposition method was related to the specific surface area of catalysts. The representative TEM images (Fig. 4) of the supported Pt catalysts are obtained to visually confirm the size distribution of Pt NPs. Pt NPs on the catalyst with smaller specific surface area such as Pt/ZnFe-MMO and Pt/NiFe-MMO showed large sizes, while monodispersed ones was observed uniformly decorated on other catalysts with smaller average sizes.

XPS characterizations were conducted to analyze the elemental composition as well as the chemical bonding environment of the Zn and Ni atoms. Fig. S3 showed a typical XPS survey spectrum for Pt/ZnFe-LDH, Pt/ZnFe-MMO, Pt/NiFe-LDH, and Pt/NiFe-MMO, respectively. The results obviously testified the presence of platinum, carbon, oxygen, iron, zinc and nickel. The both high-resolution  $\text{Zn}2\text{p}$  XPS spectrum in the Fig. 2c consisted of two asymmetric peaks assigned to the  $\text{Zn}2\text{p}_{1/2}$  and  $\text{Zn}2\text{p}_{3/2}$  core levels at eV and, which revealed that the whole Zn was in the oxidized state. A distinct difference was presented in the  $\text{Ni}2\text{p}$  region (Fig. 3d). The  $\text{Ni}2\text{p}$  spectrum for the Pt/NiFe-MMO was deconvoluted into three pairs of doublets attributed to zerovalent  $\text{Ni}^0$  and  $\text{Ni}^{2+}$  species, and two shakeup satellites. In the case of Pt/NiFe-LDH, No  $\text{Ni}^0$  contribution was recorded in the  $\text{Ni}2\text{p}$  region. The presence of zerovalent Ni in the Pt/NiFe-MMO may form PtNi alloy on the surface, which led to a higher selectivity in the fully

**Table 2** The effect of support on catalytic performance in the selective hydrogenation of CAL

Catalysts	Conv. (%)	Sele. (%)		
		HCAL	HCOL	COL
Pt/MgFe-LDH	97.9	1.4	29.5	69.2
Pt/MgFe-MMO	99.0	0.1	64.9	35.1
Pt/ZnFe-LDH	95.2	3.1	5.9	91.0
Pt/ZnFe-MMO	84.8	7.4	7.2	85.5
Pt/CoFe-LDH	51.6	22.0	6.6	71.4
Pt/CoFe-MMO	27.6	17.0	7.8	75.2
Pt/NiFe-LDH	99.3	28.2	51.3	20.4
Pt/NiFe-MMO	100.0	0	100.0	0

Reaction conditions: 8.2 mmol CAL, 19.0 mL  $\text{C}_2\text{H}_5\text{OH}$ , 60 °C, 2.0 MPa, 0.1 g catalyst, 2 h.

hydrogenated product than Pt/NiFe-LDH did (shown in Table 2 and Table 3)

Table 2 lists the catalytic performance of CAL hydrogenation over the various Fe-based LDH and derived MMO supported Pt catalysts. The support effect of LDH and derived MMO is strongly dependent on the metal elements. Firstly, trivalent element dominates the catalytic performance of different LDHs. There is no doubt that Fe-based support exhibits an improvement in both activity and selectivity than Al-based support. Divalent species also have a significant influence on the activity and selectivity. Clearly, Pt/ZnFe-LDH catalyst showed best selectivity in COL with a high conversion of 95.2 % compared with the other catalysts under the same reaction conditions. Although the high conversion is achieved over Mg-based and Ni-based LDH and MMO supported catalyst, the poor selectivity was obtained simultaneously. Specially, the hydrogenation over Pt/NiFe-MMO catalyst afforded a complete conversion into HCOL. It was well known that Ni-containing catalyst favored the hydrogenation of the  $\text{C}=\text{C}$  group and Fe-containing catalyst was in favour of the  $\text{C}=\text{O}$  group hydrogenation, which lead to the complete hydrogenation mostly attributed to “synergetic effect” between the Ni and Fe element. However, Co-containing Pt/CoFe-MMO catalyst showed poor activity due to its magnetic property, which limited the dispersion of catalyst in the magnetic stirring reaction. Fig. S5a shows the result of the selective hydrogenation of CAL as a function of reaction time over the optimal Pt/ZnFe-LDH. The reaction time sharply influenced the conversion of CAL, which was improved significantly with time increase and reached nearly 90% in 100 min. CAL is almost completely converted in 140 min, and a relatively high selectivity to COL was gained kept constant during the whole reaction process.

The relatively satisfied catalysts in the CAL hydrogenation were employed in the hydrogenation reactions of citral. The hydrogenation reactions of citral were usually performed above 100 °C.<sup>22-24</sup> In this work, the reaction was carried out at a relatively low temperature 70 °C. Unfortunately, Pt/ZnFe-LDH lost the excellent catalytic performance and other catalyst presented the similar result (Table 3 and Table S1). However,

**Table 3** The effect of support on catalytic performance in the selective hydrogenation of CAL

Catalysts	Conv. (%)	Sele. (%)			
		Citronellal	DOL	Citronellol	UALC
Pt/NiFe-LDH	100.0	0.0	8.1	89.8	2.1
Pt/NiFe-MMO	100.0	0.0	32.4	67.6	0.0
Pt/ZnFe-LDH	15.8	11.3	0.0	14.2	74.5
Pt/ZnFe-MMO	10.7	12.7	0.0	10.1	77.2

Reaction conditions: 5.8 mmol Citral, 19.0 mL C<sub>2</sub>H<sub>5</sub>OH, 70 °C, 2.0 MPa, 0.1 g catalyst, 2 h.

extremely superior activity was obtained over the NiFe-LDH and NiFe-MMO supported catalysts. It implied that divalent species, Ni, played an important role on the reaction. The lowered repulsive forces existing between the d orbitals of nickel and the reactants improved the adsorption of citral and hydrogen molecules on the catalyst, resulting in the high activity of Ni-based LDH and MMO supported catalysts.<sup>23</sup> According to the catalytic performance of the catalysts, we selected the Pt/NiFe-LDH catalyst to study the influence of time (Fig. S5b). The reaction over the Pt/NiFe-LDH catalyst was very active and around 80% conversion was achieved after just 10 min. And citral was almost completely converted after 30 min. the conjugated C=C bond and C=O bond in citral was preferentially and rapidly reduced to produce citronellal and unsaturated alcohols (geraniol and nerol, UALC), respectively at the initial reaction time of about 10 min. The result implied that the hydrogenation of C=C and C=O bonds take place nearly in parallel over the Pt/NiFe-LDH and the hydrogenation of C=C bond was a little more easily performed than that of C=O bond. Simultaneously, the consecutive hydrogenation of citronellal and UALC led to a rapid increase of citronellol, which reached the highest value in 80 min. The selectivity of citronellol decreased when the reaction time was extended, because the citronellol was converted to 3, 7-dimethyloctanol (DOL) via the further hydrogenation of the single C=C bond.

The stability of the catalyst was evaluated by recycling experiment. The results were similar to previous research. For the CAL hydrogenation over the Pt/ZnFe-LDH catalyst (Fig. S6), it is noted that the conversion slightly decreased as the recycle times increased and the good catalytic activity was still achieved after the fourth run. The COL selectivity had a sharp decrease mostly owing to an oxidation of active Pt on the catalysts. Before the fifth run, the catalyst was reduced with NaBH<sub>4</sub> and regained the high selectivity toward COL. The similar phenomenon was observed in the case of Pt/NiFe-LDH catalyst in the citral hydrogenation reaction (Fig. S7).

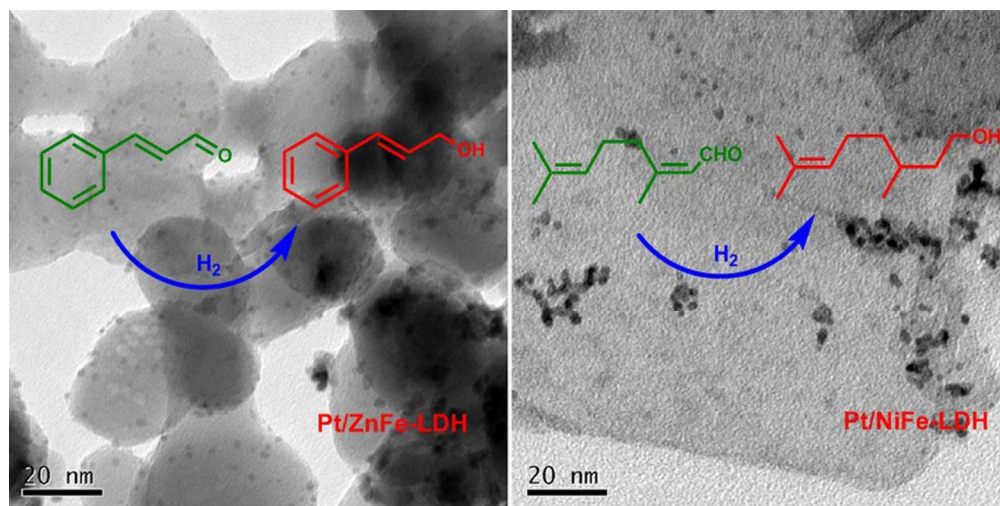
In summary, we successfully fabricated Fe-based LDH and derived MMO supported Pt catalysts. The catalysts were employed for the selective hydrogenation of CAL and citral. Compared with Al-based support, Fe-based support exhibited an improvement in both activity and selectivity. Divalent species also had a significant influence on the activity and selectivity. Among the catalysts, Pt/ZnFe-LDH showed the best activity and selectivity for the

hydrogenation of C=O bond in the CAL and citral was mostly transformed into citronellol over the Pt/NiFe-LDH catalyst.

The authors gratefully acknowledge financial support from the National Natural Science Foundation of China (No. 21203113).

## Notes and references

- H. G. Manyar, B. Yang, H. Daly, H. Moor, S. McMonagle, Y. Tao, G. D. Yadav, A. Goguet, P. Hu and C. Hardacre, *ChemCatChem*, 2013, **5**, 506-512.
- J. Zhu, M. Li, M. Lu and J. Zhu, *Catal. Sci. Tech.*, 2013, **3**, 737-744.
- X. Yang, D. Chen, S. Liao, H. Song, Y. Li, Z. Fu and Y. Su, *J. Catal.*, 2012, **291**, 36-43.
- W. Lin, H. Cheng, L. He, Y. Yu and F. Zhao, *J. Catal.*, 2013, **303**, 110-116.
- Q. Yu, X. Zhang, B. Li, J. Lu, G. Hu, A. Jia, C. Luo, Q. Hong, Y. Song and M. Luo, *J. Mol. Catal. A: Chem.*, 2014, **392**, 89-96.
- K. Taniya, H. Jinno, M. Kishida, Y. Ichihashi and S. Nishiyama, *J. Catal.*, 2012, **288**, 84-91.
- Y. Zhu and F. Zaera, *Catal. Sci. Tech.*, 2014, **4**, 955-962.
- J. Serrano-Ruiz, A. López-Cudero, J. Solla-Gullón, A. Sepúlveda-Escribano, A. Aldaz and F. Rodríguez-Reinoso, *J. Catal.*, 2008, **253**, 159-166.
- Z. Guo, C. Xiao, R. V. Maligal-Ganesh, L. Zhou, T. W. Goh, X. Li, D. Tesfagaber, A. Thiel and W. Huang, *ACS Catal.*, 2014, **4**, 1340-1348.
- Z. Liu, X. Tan, J. Li and C. Lv, *New J. Chem.*, 2013, **37**, 1350-1357.
- P. Concepción, Y. Pérez, J. Hernandez-Garrido, M. Fajardo, J. Calvino and A. Corma, *Phys. Chem. Chem. Phys.*, 2013, **15**, 12048-12055.
- J. Zhao, M. Shao, D. Yan, S. Zhang, Z. Lu, Z. Li, X. Cao, B. Wang, M. Wei and D. G. Evans, *J. Mater. Chem. A*, 2013, **1**, 5840-5846.
- X. Xiang, W. He, L. Xie and F. Li, *Catal. Sci. Tech.*, 2013, **3**, 2819-2827.
- J. Feng, C. Ma, P. J. Miedziak, J. K. Edwards, G. L. Brett, D. Li, Y. Du, D. J. Morgan and G. J. Hutchings, *Dalton Transactions*, 2013, **42**, 14498-14508.
- Z. Sun, L. Jin, S. He, Y. Zhao, M. Wei, D. G. Evans and X. Duan, *Green Chemistry*, 2012, **14**, 1909-1916.
- Z. Tian, Q. Li, J. Hou, L. Pei, Y. Li and S. Ai, *J. Catal.*, 2015, **331**, 193-202.
- W. O. Oduro, N. Cailuo, K. M. K. Yu, H. Yang and S. C. Tsang, *Phys. Chem. Chem. Phys.*, 2011, **13**, 2590-2602.
- M. Englisch, V. S. Ranade and J. A. Lercher, *J. Mol. Catal. A: Chem.*, 1997, **121**, 69-80.
- X. Xiang, H. I. Hima, H. Wang and F. Li, *Chem. Mater.*, 2007, **20**, 1173-1182.
- S. A. B. Asif, S. B. Khan and A. M. Asiri, *Nanoscale Res. Lett.*, 2014, **9**, 1-9.
- K. Parida and L. Mohapatra, *Chem. Eng. J.*, 2012, **179**, 131-139.
- H. Daly, H. Manyar, R. Morgan, J. M. Thompson, J.-J. Delgado, R. Burch and C. Hardacre, *ACS Catal.*, 2014, **4**, 2470-2478.
- L. Yang, Z. Jiang, G. Fan and F. Li, *Catal. Sci. Tech.*, 2014, **4**, 1123-1131.
- A. Vicente, G. Lafaye, C. Especel, P. Marécot and C. T. Williams, *J. Catal.*, 2011, **283**, 133-142.



112x56mm (300 x 300 DPI)